

# Underactuated Finger Mechanism Using Contractible Slider-Crank and Stackable Four-Bar Linkages

Dukchan Yoon, *Student Member, IEEE*, and Youngjin Choi<sup>ID</sup>, *Senior Member, IEEE*

**Abstract**—This paper presents an underactuated finger mechanism that is able to conduct both self-adaptive grasping and natural motions, such as flexion and extension. The robotic finger is realized with a three degrees-of-freedom mechanism composed of stackable four-bar linkages and contractible slider-cranks having a linear spring in each mechanism layer. Kinematics and static force analysis are performed to reveal the operation principle of the proposed finger mechanism. The procedure for synthesizing the linkages is also suggested using Freudenstein's equation. Finally, both simulations and experiments are conducted to confirm the design feasibility.

**Index Terms**—Grasping, robot kinematics, underactuation.

## NOMENCLATURE

$t$	Slider offset.
$s$	Stroke length of linear actuator.
$r$	Moving distance of slider.
$l_{iA}$	Length of segment $AC_i$ for $i = 1, 2, 3$ .
$l_{iB}$	Length of segment $BC_i$ for $i = 1, 2, 3$ .
$l'_{iB}$	Length of segment $C_i C'_i$ for $i = 1, 2, 3$ .
$l_{iC'}$	Length of segment $C'_i E_i$ for $i = 2, 3$ .
$l_{iD'}$	Length of segment $E_i D'$ for $i = 2, 3$ .
$l'_{iD'}$	Length of segment $E_i E'_i$ for $i = 2, 3$ .
$l_{iE'}$	Length of segment $E'_i F_i$ for $i = 2, 3$ .
$l_{iD}$	Length of segment $F_i D$ for $i = 2, 3$ .
$l'_{3D}$	Length of segment $F_3 F'_3$ .
$l_{3F'}$	Length of segment $F'_3 H_3$ .
$l_G$	Length of segment $H_3 G$ .
$l_i$	Length of proximal, middle, and distal phalanx for $i = 1, 2, 3$ , respectively.

Manuscript received January 24, 2017; revised May 16, 2017; accepted June 28, 2017. Date of publication July 4, 2017; date of current version October 13, 2017. Recommended by Technical Editor H. A. Varol. This work was supported by the Convergence Technology Development Program for Bionic Arm through the National Research Foundation of Korea funded by the Ministry of Science, ICT, and Future Planning, South Korea, under Grant NRF-2015M3C1B2052811. (*Corresponding author: Youngjin Choi*.)

The authors are with the Department of Electronic Systems Engineering, Hanyang University, Ansan 15588, South Korea (e-mail: dcyon@hanyang.ac.kr; cyj@hanyang.ac.kr).

Color versions of one or more of the figures in this paper are available online at <http://ieeexplore.ieee.org>.

Digital Object Identifier 10.1109/TMECH.2017.2723718

$\psi_{iA}$	Angles b/w link $l_{iA}$ and X-axis for $i = 1, 2, 3$ (b/w indicates between).
$\psi_{iB}$	Angles b/w link $l_{iB}$ and X-axis for $i = 1, 2, 3$ .
$\psi_{iC'}$	Angles b/w link $l_{iC'}$ and X-axis for $i = 2, 3$ .
$\psi_{iD'}$	Angles b/w link $l_{iD'}$ and X-axis for $i = 2, 3$ .
$\psi_{iE'}$	Angles b/w link $l_{iE'}$ and X-axis for $i = 2, 3$ .
$\psi_{iD}$	Angles b/w link $l_{iD}$ and X-axis for $i = 2, 3$ .
$\psi_{3F'}$	Angle b/w link $l_{3F'}$ and X-axis.
$\psi_{3G}$	Angle b/w link $l_{3G}$ and X-axis.
$u_{Ci}$	Transmission angle b/w link $l_{iG}$ and $l_{iB}$ for $i = 1, 2, 3$ .
$u_{Ei}$	Transmission angle b/w link $l_{iC'}$ and $l_{iD'}$ for $i = 2, 3$ .
$u_{Fi}$	Transmission angle b/w link $l_{iE'}$ and $l_{iD}$ for $i = 2, 3$ .
$u_{H_3}$	Transmission angle b/w link $l_{3F'}$ and $l_{3G}$ .
$\theta_i$	Rotational angle of link $l_i$ for $i = 1, 2, 3$ .
$\vec{q}$	Vector of input displacement.
$\vec{p}_i$	Vector of contact position for $i = 1, 2, 3$ .
$h_i$	Distance b/w contact point and joint of each phalanx.
$\vec{f}_i$	Vector of grasping force exerted to each phalanx.
$\vec{f}_d$	Vector of driving force.
$\vec{f}_e$	Vector of external force.
$J_p, J_q, J$	Jacobian matrices.
$\varphi_i$	Angle of $f_i$ calculated from X-axis for $i = 1, 2, 3$ .
$k_i$	Stiffness of spring for $i = 1, 2$ .
$m_r$	Initial and final distances of slider for $m = o, e$ .
$m\psi_{iB}$	Initial and final angles of slider for $m = o, e$ .
$m\psi_{2D'}$	Initial and final angles of link $l_{2D'}$ for $m = o, e$ .
$\varepsilon_i$	Constant coefficient in terms of link parameters.
$z'$	Transmission defect.

## I. INTRODUCTION

THE HAND is one of the most important parts in the human body for physical interactions with the environments. Many researchers have tried to develop robotic hands able to mimic dexterous human hand movements, such as grasping, pinching, and other versatile motions. In order to achieve sufficient dexterity, several robotic hands have been developed; for instance, the Utah/Massachusetts Institute of Technology (MIT) hand operated by tendons with 16 degrees of freedom (DOFs) in [1], the University of Bologna (UB) hand III operated by pulling tendons via elastic joints with 16 DOFs in [2], the Keio hand operated by elastic elements and ultrasonic motors with 20 DOFs in [3], the anatomically correct testbed

(ACT) hand operated by a human-like tendon structure with 21 DOFs in [4], and the German Aerospace Center (DLR) hand operated by tendons with 19 DOFs in [5]. These examples have been developed as fully actuated hand systems, and their finger mechanisms have three DOFs operated by three actuators. It should be noted that the number of actuators is referred to as degrees-of-actuator (DOAs) in this paper. Most fully actuated hands are driven by the tendons, because robotic hands can be easier to design in such a way that the tendon-drive actuators are located in the forearm. However, in order to realize the aforementioned desired motions, such as grasping, pinching, and expressing various hand gestures, the result will be bulky and heavy, because many actuators and sensors are required to drive each phalanx in the robotic finger.

Over the last few decades, many researchers have been devoted to designing a simpler and more effective finger mechanism. Rodriguez *et al.*, Dechev *et al.*, and Didrick have presented finger mechanisms composed of three phalanges with a transmission system in [6]–[8], respectively. The phalanges are implemented by coupling four-bar linkages as the transmission system to reduce the number of both DOFs and DOAs at the same time. When an actuator is operated, three phalanges are simultaneously flexed or extended. In other words, it has one DOF and one DOA. Its main feature is to realize human-like flexion and extension with the fixed ratio between rotational angles prescribed by the length parameters of the linkage. However, this kind of the mechanism has difficulty in grasping or enveloping arbitrary objects with different shapes and sizes because its one DOF is fully constrained by the first contact with an object.

In order to improve the ability to grasp an object, the concept of underactuation is often applied to the finger mechanism. Underactuation means to reduce DOAs without affecting DOFs by using passive elements, such as springs and mechanical limits as mentioned in [9]–[11]. This approach leads the finger to have the capability of self-adaptation without any help from a control algorithm when the object is grasped. Laliberté and Gosselin have proposed an underactuated finger with two DOFs in [9]. A torsional spring is installed into the mechanism so that the phalanx can maintain extension (or the initial configuration) during the movement. When the proximal phalanx makes the first contact with an object, the input actuation force is increased to overcome the spring torque, and then the distal phalanx starts rotating toward the second contact. This research was extended into three DOFs in [12]. However, these studies focused on only grasping and pinching to grip an object, which are far from the human-like finger motions that include flexion and extension.

In contrast, Hirano *et al.* have compared the grasping performance between fingers with caging and noncaging motions and revealed the importance of the caging motion in grasping dynamic objects in [13]. In order to realize this motion, torsional springs are installed into each joint of a multilink finger. However, the range of motion (ROM) and elasticity of each spring need to be carefully considered according to the finger movement, because the springs are placed into the working joints.

Using a similar approach to [6]–[8], in our previous work, Jang *et al.* have suggested a robotic index finger prosthesis with three phalanges in [14]. This study has shown that the prosthesis is able to imitate flexion and extension. In order to activate the

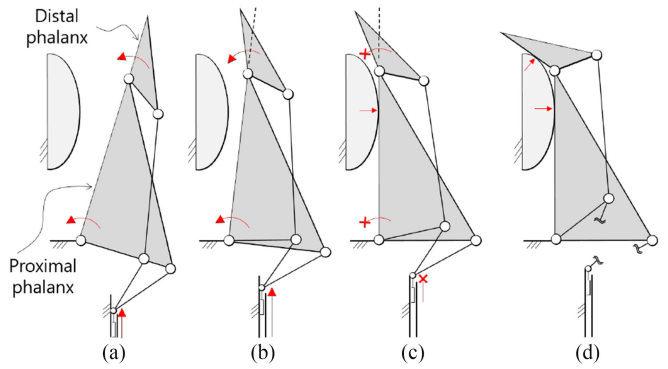


**Fig. 1.** Basic concept of the stackable four-bar linkages mechanism: (a) and (b) the human-like flexion sequence proposed in [14]; (c) its main drawback that it can no longer move while in contact with the object; and (d) the self-adaptive grasping presented in this paper.

three phalanges with one actuator, a stacked set of four-bar linkages was used to reduce the number of DOFs to one (the number of DOAs). Fig. 1 illustrates the basic concept of the finger mechanism proposed in [14] and its motion sequence. Before contact with the object, two phalanges are simultaneously flexed by the stacked four-bar linkages when a linear actuator is working, as shown in Fig. 1(a) and (b). After the proximal phalanx makes contact with the object, the distal phalanx can no longer move because the mechanism is stuck, as depicted in Fig. 1(c). Thus, this finger was only able to accomplish a limited grasping task. In this paper, we are to extend the finger mechanism proposed in [14] into an underactuated system utilizing elastic elements. Ultimately, it will have three DOFs and one DOA. The mechanism proposed in this paper can perform human-like flexion and extension without any deformation of the spring as well as the self-adaptive grasping suggested in Fig. 1(d). It should be noted that the distal phalanx does not have constant orientation while pinching the object, which is different from the SARAH hand suggested in [12].

This paper is organized as follows: the definition of natural motion, mechanism design, and its operation principle are described in Section II, kinematics and static force analysis are given in Section III, the procedure for synthesizing the linkages is proposed in Section IV, the effectiveness of the proposed mechanism is verified through simulations and experiments in Section V, and finally, we draw conclusions in Section VI.

## II. DESIGN OF FINGER MECHANISM

Stackable four-bar mechanisms connected to three slider-cranks have been used for several robotic applications such as the prosthetic index finger in [14] and the manipulators in [15] and [16]. The difference between the former and the latter was the number of actuators used to control the transmission system. The slider-cranks utilized in the latter were independently actuated by three actuators for implementing three DOFs, while in the former they were simultaneously actuated by only one actuator for implementing one DOF. For the former, three slider joints were tied together. In these previous works, the slider-cranks were used to deliver input forces to the stacked mechanism layers. If a rotary actuator is used, it is possible to

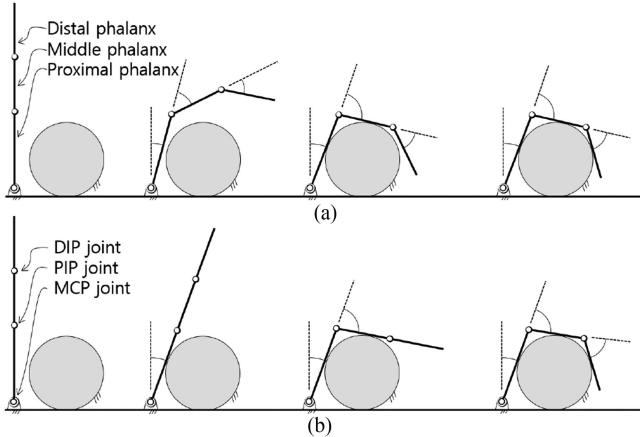


**Fig. 2.** Comparison between preshaping and nonpreshaping in the underactuated fingers: (a) preshaping; and (b) nonpreshaping.

replace the slider-crank with another input mechanism such as the worm-gear mentioned in [16]. In this section, we will focus on how to design and actuate three slider-cranks for implementation of underactuation with practical considerations, such as the type of elastic element, its location separated from the working joint, and the volumetric size of the system. To begin, the definition of natural finger motion is suggested in the following section.

#### A. Definition of Natural Motion of the Finger

There may not be any formal definition of natural finger motion. However, through literature surveys, we can understand the natural motion in terms of three properties: preshaping before grasping; the linear relationship between the movements of the phalanges; and human phalanx size and ROM.

First of all, Higashimori *et al.* have emphasized the significance of preshaping when grasping the cylindrical object in [17]. Fig. 2 illustrates the comparison between preshaping and nonpreshaping in the underactuated fingers. In Fig. 2(a), the cylindrical object is caged by three phalanges in advance, and then adaptive grasping is achieved. This sequence is similar to human fingers. The caging motion mentioned in [13] was also referred to as preshaping motion. In contrast, a nonpreshaping finger is not flexed until it is in contact with the object because the finger maintains extension, as shown in the Fig. 2(b). As presented in [13] and [17], this may cause the object to slide away, and thus grasping will fail.

Figliolini and Ceccarelli have dealt with natural movements of the finger, such as flexion and extension, in [18]. It was argued that the flexion of each phalanx is not completely independent when the human finger performs the closing motion. Indeed, this movement has an approximately linear relationship between phalanges as follows:

$$\theta_2 = \lambda_1 \theta_1 \quad \text{and} \quad \theta_3 = \lambda_2 \theta_1 \quad (1)$$

where  $\theta_1$ ,  $\theta_2$ , and  $\theta_3$  are the angles of the proximal, middle, and distal phalanges, respectively, and  $\lambda_1$  and  $\lambda_2$  are the proportional constants that differ from individual to individual.

Last, Kapandji has discussed the ROMs with respect to human finger movement in [19]. For the middle finger, the ROM of the metacarpophalangeal joint is slightly smaller than  $90^\circ$ , the proximal interphalangeal joint is greater than  $90^\circ$ , and the distal interphalangeal joint is also slightly smaller than  $90^\circ$ . Stillfried *et al.* also concurred with these arguments in [20] based on their measurement data. In this paper, it is defined that the finger motion is natural when the above three specifications are satisfied.

#### B. Mechanism Design

The underactuated finger mechanism proposed here is composed of three phalanges by using stackable four-bar linkages. In detail, Fig. 3(a)–(c) illustrates mechanism layers for three phalanges; Fig. 3(a) shows the first slider-crank input linkage connected with a linear spring for the proximal phalanx, Fig. 3(b) shows the second slider-crank input linkage connected with a linear spring as well as four-bar linkages for the middle phalanx, and Fig. 3(c) shows the common slider-crank and four-bar linkages for the distal phalanx. All the mechanism layers are stacked in parallel, sharing several common joints  $O$ ,  $A$ ,  $B$ ,  $D$ ,  $D'$ , and  $G$ . Furthermore, joints  $O$  and  $B$  are fixed to the ground. Ternary links  $C_1BD$ ,  $F_2DG$ , and  $H_3GI$  are referred to as the proximal, middle, and distal phalanges, respectively. Two four-bar linkages share the longest link  $BD$  in the mechanism layers, in order to appropriately design the lengths of the input and output links. It is again noted that all the mechanism layers are driven by only one linear actuator along the  $X_0$  axis through three slider-cranks at the same time. However, the posture of the finger can be reconfigured as the linear springs in links  $l_{1A}$  and  $l_{2A}$  are deformed.

#### C. Operation Principle of Underactuation

Fig. 3(d) and (f) illustrate the operation principle of the proposed three slider-cranks. In these figures, links  $l_{iB}$  for  $i = 1, 2, 3$  on joint  $B$  fixed to the ground are rotated in the clockwise direction as the actuated joint  $A$  moves from the initial position  $O$  along the  $X_0$  axis; that is, the distance  $r$  decreases along the dashed line, as shown in the Fig. 3(d). When the output link  $BD$  is stuck by an object, the  $l_{1B}$  link is fixed, but joint  $A$  can further translate along the dashed line. Both links  $l_{2B}$  and  $l_{3B}$  continue to be rotated because the linear spring in link  $l_{1A}$  can be contracted, as illustrated in Fig. 3(e). In the same way, Fig. 3(f) illustrates that link  $l_{3B}$  can be rotated on joint  $B$  due to continuous contractions of the two springs in links  $l_{1A}$  and  $l_{2A}$  even though links  $l_{1B}$  and  $l_{2B}$  stop rotating. For these reasons, the proposed finger mechanism has the property of underactuation, and it can also perform both natural motion and self-adaptive grasping.

### III. KINEMATICS AND STATICS

Kinetostatic analysis of underactuated finger has been introduced in [21] and applied to our mechanism for evaluating the grasp force. Kinematic parameters are described graphically in Fig. 3. It should be noted that the base coordinate system is attached at origin  $O$ , and the absolute coordinate

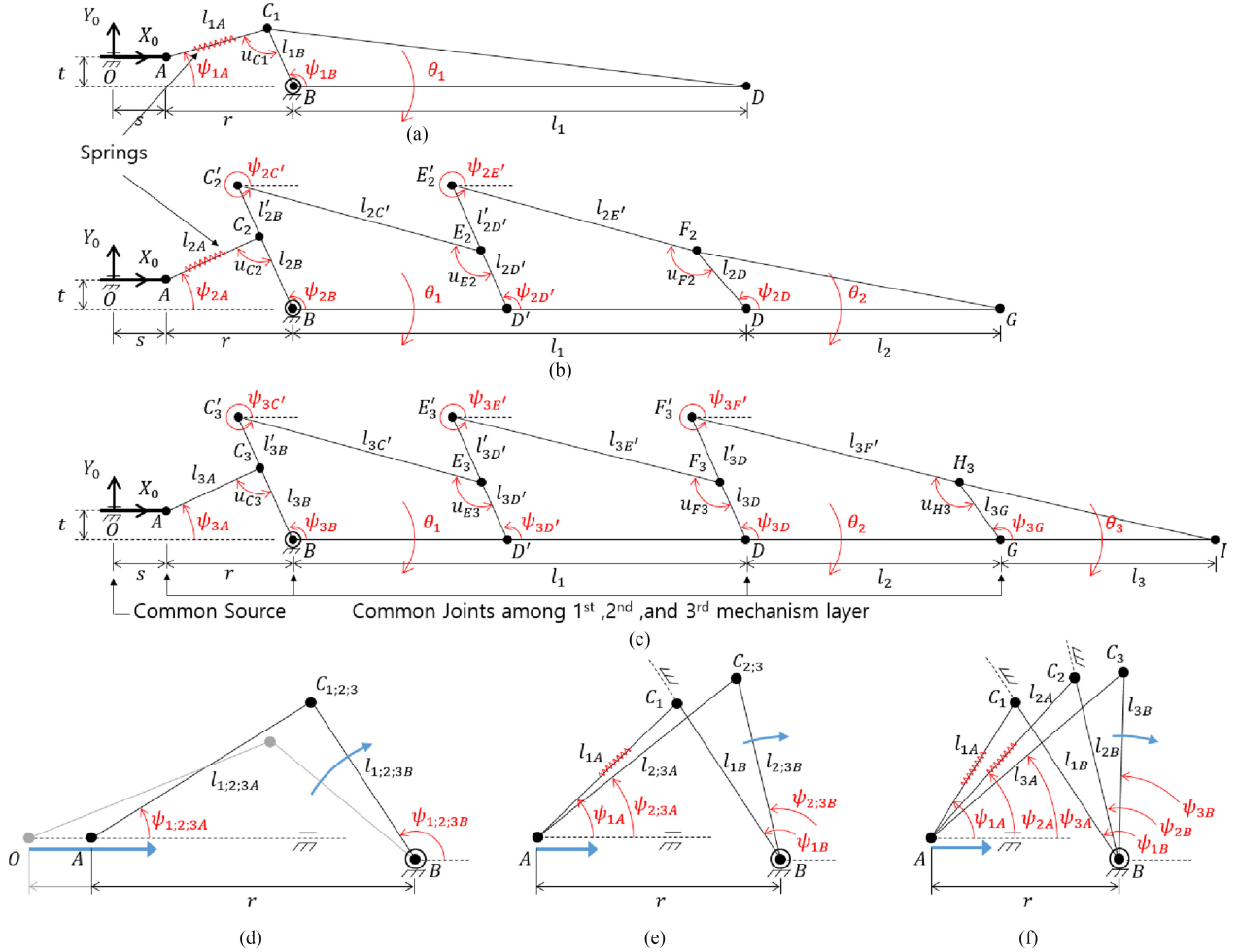


**Fig. 3.** Schematic structure of the proposed finger mechanism: (a) first mechanism layer; (b) second mechanism layer; and (c) third mechanism layer. The operation principle of underactuation with the proposed three slider-cranks and two linear springs when the linear actuator is working: (d) the actuated joint  $A$  moves from initial position  $O$  along the  $X_0$  axis; (e) both links  $l_{2B}$  and  $l_{3B}$  continue to be rotated while the linear spring in link  $l_{1A}$  is contracted; and (f) link  $l_{3B}$  can be rotated on joint  $B$  due to continuous contractions of the two springs in links  $l_{1A}$  and  $l_{2A}$  even though links  $l_{1B}$  and  $l_{2B}$  stop rotating.

is applied to all joints.  $\psi_{im}$  expresses the angle from the  $X_0$  axis to the  $m$ th link in the  $i$ th mechanism layer, where  $i = 1, 2, 3$  and  $m = A, B, C', D', E', F', G$ . The proximal, middle, and distal angles denoted by  $\theta_i$  from the  $X_0$  axis to links  $l_1$ ,  $l_2$ , and  $l_3$ , respectively, are represented as

$$\begin{aligned} \theta_1 &= \psi_{1B} - {}^o\psi_{1B} \\ \theta_2 &= \psi_{2D} - {}^o\psi_{2D} \\ \theta_3 &= \psi_{3G} - {}^o\psi_{3G} \end{aligned} \quad (2)$$

where  ${}^o\psi_{1B}$ ,  ${}^o\psi_{2D}$ , and  ${}^o\psi_{3G}$  denote the initial constant angles of the proximal, middle, and distal phalanges, respectively, when the phalanges are extended straight.

#### A. Jacobian

In order to determine the velocity relationship between the input and the output, the loop closure equation of the three slider-crank  $AC_iB$  is expressed as

$$l_{iA} e^{j\psi_{iA}} = t e^{j\frac{3}{2}\pi} + r + l_{iB} e^{j\psi_{iB}} \quad \text{for } i = 1, 2, 3 \quad (3)$$

where  $t$  is the slider offset in the  $Y_0$  direction from joint  $B$  to  $O$ . After taking the time differentiation and rearranging (3), we have

$$\begin{bmatrix} \dot{\psi}_{iA} \\ \dot{\psi}_{iB} \end{bmatrix} = G_{i1}^{-1} K_{i1} \begin{bmatrix} \dot{r} \\ \dot{l}_{iA} \end{bmatrix} \quad \text{for } i = 1, 2, 3 \quad (4)$$

where

$$G_{i1} = \begin{bmatrix} -l_{iA} s_{iA} & l_{iB} s_{iB} \\ l_{iA} c_{iA} & -l_{iB} c_{iB} \end{bmatrix} \quad \text{for } i = 1, 2, 3$$

$$K_{i1} = \begin{bmatrix} 1 & -c_{iA} \\ 0 & -s_{iA} \end{bmatrix} \quad \text{for } i = 1, 2 \quad \text{and} \quad K_{31} = \begin{bmatrix} 1 & 0 \\ 0 & 1 \end{bmatrix}.$$

It should be noted that  $K_{31}$  is an identity matrix since  $l_{3A}$  is not a variable in contrast with  $l_{1A}$  and  $l_{2A}$ . For notational ease, the sinusoidal functions are expressed as  $c_{im} = \cos \psi_{im}$  and  $s_{im} = \sin \psi_{im}$ . Here, we can obtain an angular velocity  $\dot{\theta}_1 (= \dot{\psi}_{1B})$  of the proximal phalanx by letting  $i = 1$  in (4).

In the same way, the loop closure equations of the double four-bar linkages  $BC'_iE_iD'$  and  $D'E'_iF_iD$  for  $i = 2,3$  connected to the slider-cranks in the second and third mechanism layers are expressed in the following forms, respectively

$$L_{iB}e^{j\psi_{iB}} + l_{iC'}e^{j\psi_{iC'}} = \frac{l_1}{2}e^{j\theta_1} + l_{iD'}e^{j\psi_{iD'}} \quad (5)$$

$$L_{iD'}e^{j\psi_{iD'}} + l_{iE'}e^{j\psi_{iE'}} = \frac{l_1}{2}e^{j\theta_1} + l_{iD}e^{j\psi_{iD}} \quad (6)$$

where  $L_{iB} = l_{iB} + l'_{iB}$  and  $L_{iD'} = l_{iD'} + l'_{iD'}$ . By applying similar procedures, we have the following equations:

$$\begin{bmatrix} \dot{\psi}_{iC'} \\ \dot{\psi}_{iD'} \end{bmatrix} = G_{i2}^{-1}K_{i2} \begin{bmatrix} \dot{\theta}_1 \\ \dot{\psi}_{iB} \end{bmatrix} \quad \text{and} \quad \begin{bmatrix} \dot{\psi}_{iE'} \\ \dot{\psi}_{iD} \end{bmatrix} = G_{i3}^{-1}K_{i3} \begin{bmatrix} \dot{\theta}_1 \\ \dot{\psi}_{iD'} \end{bmatrix} \quad (7)$$

for  $i = 2,3$ , where

$$\begin{aligned} G_{i2} &= \begin{bmatrix} -l_{iC'}s_{iC'} & l_{iD'}s_{iD'} \\ l_{iC'}c_{iC'} & -l_{iD'}c_{iD'} \end{bmatrix} & K_{i2} &= \begin{bmatrix} -\frac{l_1}{2}s_{1B} & L_{iB}s_{iB} \\ \frac{l_1}{2}c_{1B} & -L_{iB}c_{iB} \end{bmatrix} \\ G_{i3} &= \begin{bmatrix} -l_{iE'}s_{iE'} & l_{iD}s_{iD} \\ l_{iE'}c_{iE'} & -l_{iD}c_{iD} \end{bmatrix} & K_{i3} &= \begin{bmatrix} -\frac{l_1}{2}s_{1B} & L_{iD'}s_{iD'} \\ \frac{l_1}{2}c_{1B} & -L_{iD'}c_{iD'} \end{bmatrix}. \end{aligned}$$

The angular velocity  $\dot{\theta}_2$  ( $= \dot{\psi}_{2D}$ ) of the middle phalanx is obtained from (7) by letting  $i = 2$ .

One four-bar linkage equipped onto link  $l_2$  in the third mechanism layer is also expressed as follows:

$$L_{3D}e^{j\psi_{3D}} + l_{3F'}e^{j\psi_{3F'}} = l_2e^{j\theta_2} + l_{3G}e^{j\psi_{3G}} \quad (8)$$

where  $L_{3D} = l_{3D} + l'_{3D}$ . Finally, we can obtain the angular velocity  $\dot{\theta}_3$  ( $= \dot{\psi}_{3G}$ ) of the distal phalanx after differentiating (8) in the following form:

$$\begin{bmatrix} \dot{\psi}_{3F'} \\ \dot{\psi}_{3G} \end{bmatrix} = G_{34}^{-1}K_{34} \begin{bmatrix} \dot{\theta}_2 \\ \dot{\psi}_{3D} \end{bmatrix} \quad (9)$$

where

$$G_{34} = \begin{bmatrix} -l_{3F'}s_{3F'} & l_{3G}s_{3G} \\ l_{3F'}c_{3F'} & -l_{3G}c_{3G} \end{bmatrix} \quad K_{34} = \begin{bmatrix} -l_2s_{2D} & L_{3D}s_{3D} \\ l_2c_{2D} & -L_{3D}c_{3D} \end{bmatrix}.$$

Therefore, all of the angles and angular velocities of the phalanges are calculated from (2)–(9); in other words, the relationship between the input velocities and the output angular velocities can be expressed as

$$\dot{\vec{\theta}} = J_q \dot{\vec{q}} \quad (10)$$

where  $J_q \in \mathbb{R}^{3 \times 3}$  denotes a Jacobian matrix for the transmission system,

$$\dot{\vec{\theta}} = [\dot{\theta}_1 \ \dot{\theta}_2 \ \dot{\theta}_3]^T \quad \text{and} \quad \dot{\vec{q}} = [\dot{r} \ l_{1A} \ l_{2A}]^T$$

in which  $\vec{\theta} \in \mathbb{R}^3$  is the angular displacement vector,  $\dot{\vec{\theta}}$  is its time derivative,  $\vec{q} \in \mathbb{R}^3$  is the input displacement vector, and  $\dot{\vec{q}}$  is its time derivative. From (10), the finger mechanism can be simplified as a serial-type planar manipulator having three revolute joints  $\theta_1, \theta_2$ , and  $\theta_3$ , as shown in Fig. 4.

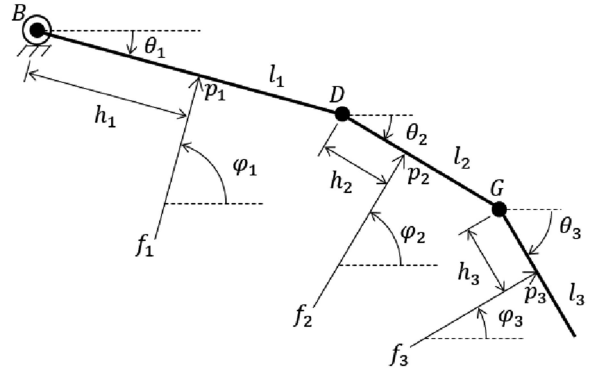


**Fig. 4.** Contact force vectors  $\vec{f}_i$  for  $i = 1,2,3$  and contact position vectors  $\vec{p}_i$  from joint  $B$  on the simplified finger mechanism, where  $\theta_1, \theta_2$ , and  $\theta_3$  denote the angles of the proximal, middle, and distal phalanges, respectively.

### B. Grasping Force

In order to calculate the grasping forces, the velocities of the contact points should be known. Let us assume that the contact points are located on each phalanx,  $l_1, l_2$ , and  $l_3$ . Referring to Fig. 4, three contact position vectors along the phalanges from joint  $B$  are expressed as

$$\begin{aligned} \vec{p}_1 &= h_1 e^{j\theta_1} \\ \vec{p}_2 &= l_1 e^{j\theta_1} + h_2 e^{j\theta_2} \\ \vec{p}_3 &= l_1 e^{j\theta_1} + l_2 e^{j\theta_2} + h_3 e^{j\theta_3} \end{aligned} \quad (11)$$

where  $h_i$  for  $i = 1,2,3$  denotes the distance from each joint of the phalanx to the contact point. If geometric information of the object is given, such as size, shape, and location, then the contact position vector  $\vec{p}_i$  can be calculated. By taking the time derivative of (11), the velocity vectors at the contact points are obtained as follows:

$$\dot{\vec{p}} = J_p \dot{\vec{\theta}}, \quad \text{where} \quad \dot{\vec{p}} = [\dot{\vec{p}}_1 \ \dot{\vec{p}}_2 \ \dot{\vec{p}}_3]^T \in \mathbb{R}^6 \quad (12)$$

and  $J_p \in \mathbb{R}^{6 \times 3}$  is a Jacobian matrix. While grasping the object, the finger might push it away in spite of preshaping. In order to calculate the grasping forces, we assume that the object is static and rigid, the object is fixed to the ground, three contact positions are known, each phalanx has only one contact point, masses and inertias of the finger are negligible, friction and gravity are ignored, forces directed toward the phalanges are considered as positive, and contact forces are normal to the surface of the lower link of each phalanx. Under the above assumptions, if the principle of virtual work is applied, then the relationship between the external force and the driving force is formulated as follows:

$$\vec{f}_a^T \dot{\vec{q}} = \vec{f}_e^T \dot{\vec{p}} \quad (13)$$

where

$$\vec{f}_a = [f_d \ f_{1A} \ f_{2A}]^T \quad \text{and} \quad \vec{f}_e = [\vec{f}_1 \ \vec{f}_2 \ \vec{f}_3]^T.$$

Here,  $f_d$  is an input force,  $f_{iA} = k_i \delta l_{iA}$  is generated by the  $i$ th linear spring having the stiffness  $k_i$  for  $i = 1,2$ . It should

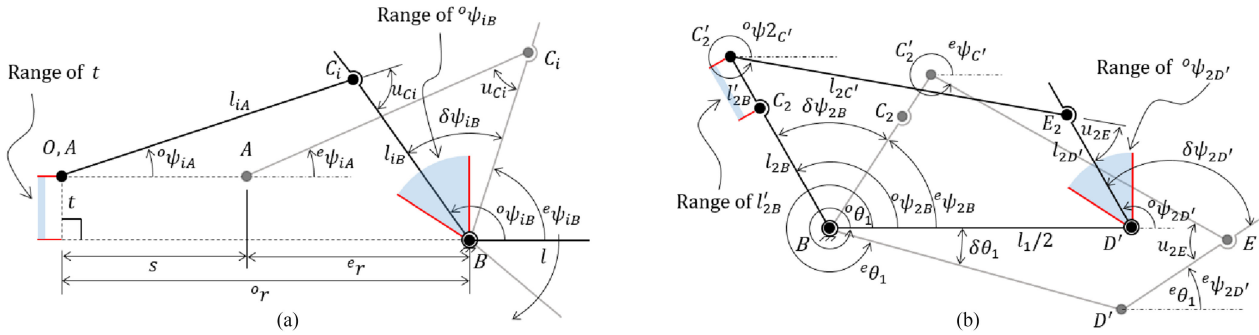


**Fig. 5.** Linkage geometries for synthesis: (a) slider-crank linkage, where  $t$  implies the slider offset,  $l_{iA}$  the coupler link length, and  $l_{iB}$  the crank link length in  $i$ th mechanism layer; and (b) four-bar linkage, where  $l'_{2B}$  implies the eccentric length in second mechanism layer.

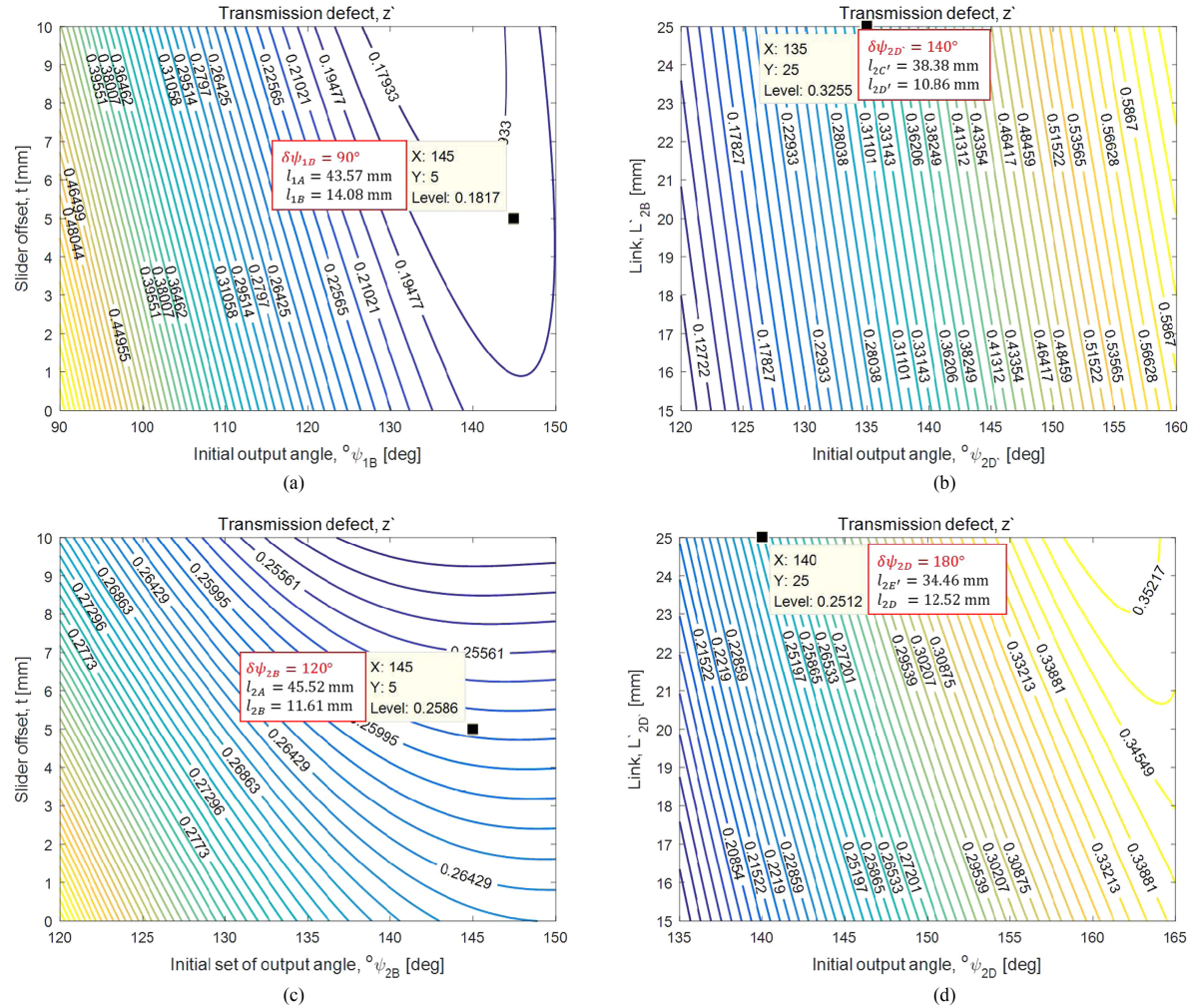


**Fig. 6.** Contours of the transmission defects: (a) slider-crank in the first mechanism layer,  $ABC_1$ ; (b) slider-crank in the second mechanism layer,  $ABC_2$ ; (c) four-bar linkage in the second mechanism layer,  $BC'E_2D'$ ; and (d) another four-bar linkage in the second mechanism layer,  $D'E_2F_2D'$ .

be noted that the  $i$ th contact force vector is defined as  $\vec{f}_i = [f_{ix}, f_{iy}]^T \in \mathbb{R}^2$  for  $i = 1, 2, 3$ , as depicted in Fig. 4.

Using (10), (12), and (13), we can obtain the relationship between the input force vector  $\vec{f}_a$  and the contact force vector  $\vec{f}_e$  as follows:

$$\vec{f}_a = J^T \vec{f}_e \quad (14)$$

where  $J = J_p J_q \in \mathbb{R}^{6 \times 3}$ . From Fig. 4, the three directional angles of  $f_i$  from the  $X_0$  axis are obtained as

$$\varphi_i = \theta_i + \frac{\pi}{2} \quad \text{for } i = 1, 2, 3. \quad (15)$$

Then,  $i$ th contact force vector can be expressed by its magnitude and angle as follows:

$$\vec{f}_{ix} = |f_i| c_i \quad \text{and} \quad \vec{f}_{iy} = |f_i| s_i \quad (16)$$

where  $s_i = \sin \varphi_i$  and  $c_i = \cos \varphi_i$ , for  $i = 1,2,3$ . Finally, (14) can be simplified as

$$\begin{bmatrix} |f_1| \\ |f_2| \\ |f_3| \end{bmatrix} = U^{-1} \begin{bmatrix} f_d \\ k_1 \delta l_{1A} \\ k_2 \delta l_{2A} \end{bmatrix} \quad (17)$$

where

$$U = \begin{bmatrix} J_{11}c_1 + J_{21}s_1 & J_{31}c_2 + J_{41}s_2 & J_{51}c_3 + J_{61}s_3 \\ J_{12}c_1 + J_{22}s_1 & J_{32}c_2 + J_{42}s_2 & J_{52}c_3 + J_{62}s_3 \\ J_{13}c_1 + J_{23}s_1 & J_{33}c_2 + J_{43}s_2 & J_{53}c_3 + J_{63}s_3 \end{bmatrix}$$

in which  $J_{ij}$  implies the  $i$ th row and  $j$ th column element of the Jacobian matrix  $J$  with respect to the proposed finger mechanism. Once the input force  $f_d$  of the linear actuator is known, two linear spring variations  $\delta l_{iA}$  for  $i = 1,2$  can be obtained from the geometric information for the grasping configuration, and then the grasping forces  $|f_1|$ ,  $|f_2|$ , and  $|f_3|$  can be determined from (17). It should also be noted that  $\delta l_{iA} = 0$  during the natural motion for  $i = 1,2$ , because there is no contact with the object.

#### IV. SYNTHESIS OF LINKAGES

For the specific design, the proposed finger mechanism is synthesized through the well-known Freudenstein's equation in [22]. Then, the transmission angles denoted as  $u_{mi}$  in Fig. 3 for  $m = C, E, F, H$  and  $i = 1,2,3$  are obtained to evaluate the force or torque transmission, considering practical design criteria, such as allowable distance between joints due to the mechanical bearing, shaft, structural collision, and suitable finger size. Freudenstein's equation with respect to all the linkages can be obtained from their kinematic models, such as (3), (5), (6), and (8). Since the synthesis procedures regarding all of the stackable mechanisms are not easily explained, we illustrate the first and second mechanism layers suggested in Fig. 3. The slider-crank and four-bar linkages shown in Fig. 5 are employed as examples to help the reader's understanding. In this figure, the solid line and the gray line are assumed to be the initial and final configurations, respectively, and their parameters are denoted by the left-superscripts "o" and "e," respectively. Some of the design parameters defined in Fig. 3(a)–(c) are predetermined; for instance, the link lengths  $l_i$  for  $i = 1,2,3$  are 50, 30, and 30 mm, respectively, referring to the human middle finger size. Their ROMs are designed so as to have the relative angular range of 0–90°.

##### A. Design of Slider-Crank Linkage

As the slider-driven joint  $A$  travels from the initial distance  ${}^o r$  to the final  ${}^e r$ , as shown in Fig. 5(a), then the crank link  $l_{iB}$  rotates on ground joint  $B$  from the initial angle  ${}^o \psi_{iB}$  to the final angle  ${}^e \psi_{iB}$ . Now, let us apply Freudenstein's equation to determine the link lengths. From (3), the kinematic model of the slider-crank, Freudenstein's equation is described as follows:

$${}^m r^2 = \varepsilon_1 + \varepsilon_2 {}^m r \cos {}^m \psi_{iB} + \varepsilon_3 \sin {}^m \psi_{iB} \quad \text{for } m = o, e \quad (18)$$

**TABLE I**  
INITIAL OUTPUT ANGLES AND THEIR TRAVEL RANGES (UNIT DEG)

$i$	${}^o \psi_{iB}$	${}^o \psi_{iD'}$	${}^o \psi_{iD}$	${}^o \psi_{iG}$	$\delta \psi_{iB}$	$\delta \psi_{iD'}$	$\delta \psi_{iD}$	$\delta \psi_{iG}$
1	145	—	—	—	90	—	—	—
2	145	135	140	—	120	140	180	—
3	145	135	135	140	120	155	235	270

**TABLE II**  
DESIGN PARAMETERS BY THE PROPOSED SYNTHESIS SCHEME (UNIT MM)

$i$	$l_i$	$l_{iA}$	$l_{iB}$	$l'_{iB}$	$l_{iC'}$	$l_{iD'}$
1	50.00	43.57	14.08	—	—	—
2	30.00	45.52	11.61	13.39	38.38	10.86
3	30.00	45.52	11.61	13.39	41.20	7.47
$i$	$l'_{iD'}$	$l_{iE'}$	$l_{iD}$	$l'_{iD}$	$l_{iF'}$	$l_{iG}$
2	14.14	34.46	12.52	—	—	—
3	17.53	36.20	11.09	8.91	38.13	9.05

where  $\varepsilon_1 = l_{iA}^2 - l_{iB}^2 - t^2$ ,  $\varepsilon_2 = -2l_{iB}$ , and  $\varepsilon_3 = 2tl_{iB}$ . From (18) and Fig. 5(a), we have seven unknowns, namely  ${}^o r$ ,  ${}^e r$ ,  ${}^o \psi_{iB}$ ,  ${}^e \psi_{iB}$ ,  $t$ ,  $l_{iA}$ , and  $l_{iB}$ . Here, three design conditions are considered: the initial distance  ${}^o r$  to secure the spring insertion,  $\delta \psi_{iB} = {}^o \psi_{iB} - {}^e \psi_{iB}$  due to the ROM of joint, and the stroke  $s = {}^o r - {}^e r$  by specification of the linear actuator. Thus, we have four unknowns to be determined through the design procedures. For example, for a given  ${}^o r$ ,  $\delta \psi_{iB}$ , and  $s$ , various link lengths of  $l_{iA}$  and  $l_{iB}$  can be determined according to various  ${}^o \psi_{iB}$  and  $t$ . In other words, whenever different  ${}^o \psi_{iB}$  and  $t$  are assigned, we can find  $l_{iA}$  and  $l_{iB}$  by solving two equation (18) obtained by applying the initial and final configurations. In contrast, when coupler  $l_{iA}$  and crank link  $l_{iB}$  are perpendicular to each other, the torque can be maximally transmitted from the input slider to the crank link. The acute angle between them is referred to as a "transmission angle" denoted by  $u_{Ci}$  in Fig. 5(a). The integration of the squared cosine function value of  $u_{Ci}$  is called the transmission defect in [23] in the following form:

$$z' = \frac{1}{s} \int_{{}^o r}^{{}^e r} \cos^2 u_{Ci} dr \quad (19)$$

where  $s = {}^o r - {}^e r$  and

$$u_{Ci} = \cos^{-1} \left( \frac{l_{iA}^2 + l_{iB}^2 - r^2 - t^2}{2l_{iA}l_{iB}} \right).$$

Choosing the minimum  $z'$  will bring about a maximum torque transmission as an average during the stroke.

In the case of the first mechanism layer,  $i = 1$ . If the design conditions are assigned to be  ${}^o r = 55$  mm,  $s = 20$  mm, and  $\delta \psi_{iB} = 90^\circ$  as the ROM of the proximal phalanx, then coupler length  $l_{iA}$  and crank length  $l_{iB}$  are calculated by the arbitrary set  $t$  and  ${}^o \psi_{iB}$  using (18), and also their transmission defects are evaluated using (19). It should be noted that the ranges of  $t$  and  ${}^o \psi_{iB}$  should be carefully chosen taking into consideration both singularity and allowable finger size. For a given  $0 \leq t \leq 10$  mm and  $90^\circ \leq {}^o \psi_{iB} \leq 150^\circ$ , we can obtain contours of the transmission defects, as shown in Fig. 6(a). The larger both  $t$  and  ${}^o \psi_{iB}$  are, the better

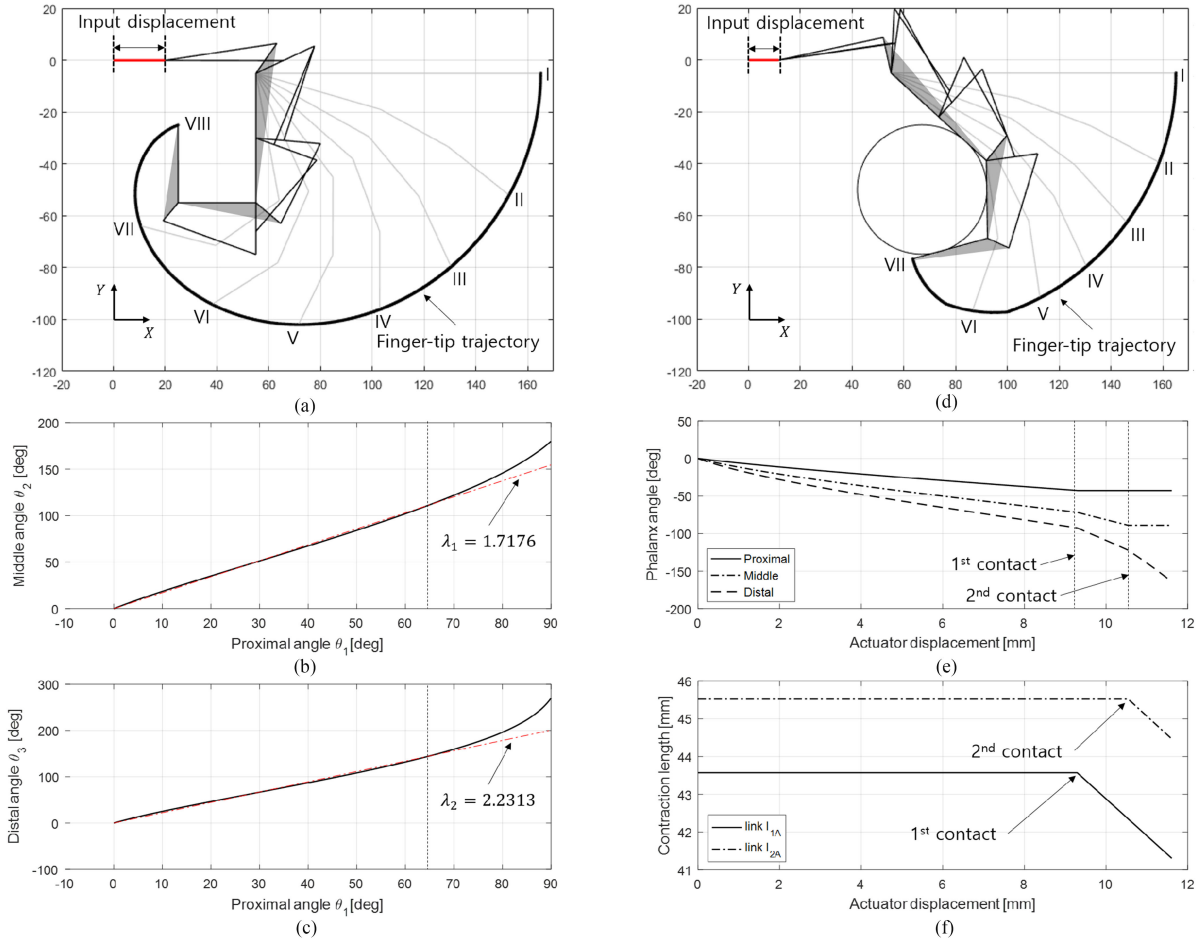


**Fig. 7.** Angles of phalanges and their approximate linear relationships during natural motion: (a) sequence of natural motion and its final configuration; (b) relationship between middle  $\theta_2$  and proximal  $\theta_1$ ; and (c) relationship between distal  $\theta_3$  and proximal  $\theta_1$ . The lengths of the spring-loaded links and the angles of the phalanges during self-adaptive grasping motion: (d) sequence of the self-adaptive grasping and its final configuration; (e) angles of the phalanges; and (f) lengths of the spring-loaded links  $l_{1A}$  and  $l_{2A}$ .

the torque transmission. If we choose  $z' = 0.1817$  considering the practical design criteria, then we obtain all the parameters, such as  $t = 5$  mm,  ${}^o\psi_{1B} = 145^\circ$ ,  $l_{1A} = 43.57$  mm, and  $l_{1B} = 14.08$  mm. In contrast, Fig. 6(b) shows the transmission defect contour for the second mechanism layer,  $i = 2$ , when  ${}^o r = 55$  mm,  $s = 20$  mm,  $t = 5$  mm, and  $\delta\psi_{2B} = 120^\circ$ . Using the same procedures, choosing  $z' = 0.2586$  in Fig. 6(b) determines the design parameters as  ${}^o\psi_{2B} = 145^\circ$ ,  $l_{2A} = 45.52$  mm, and  $l_{2B} = 11.61$  mm.

### B. Design of Four-Bar Linkage

Like the slider-crank, referring to Fig. 5(b), the four-bar linkage is synthesized by using the Freudenstein's equation. Consider the four-bar linkage in the second mechanism layer  $BC'_2E_2D'$ , the Freudenstein's equation can be obtained by using (6) as follows:

$$\cos({}^m\psi_{2D'} - {}^m\psi_{2B}) = \varepsilon_1 + \varepsilon_2 \cos({}^m\theta_1 - {}^m\psi_{2D'}) + \varepsilon_3 \cos({}^m\theta_1 - {}^m\psi_{2B}) \quad \text{for } m = o, e \quad (20)$$

where  $\varepsilon_1 = \frac{(l_1/2)^2 + l_{2D'}^2 + L_{2B}^2 - l_{2C'}^2}{2l_{2D'}L_{2B}}$ ,  $\varepsilon_2 = \frac{l_1}{2L_{2B}}$ , and  $\varepsilon_3 = -\frac{l_1}{2l_{2D'}}$ . In the second mechanism layer, since the four-bar linkage is connected to the slider-crank around joint  $C_2$  in Fig. 5, the output angle of the slider-crank can be used as the operating input angle of the four-bar linkage. Thus, the input angles,  ${}^o\psi_{2B}$  and  $\delta\psi_{2B}$ , are given as  $145^\circ$  and  $120^\circ$ , respectively. From the design of the slider-crank, the crank length  $l_{2B} = 14.08$  mm. From the link length  $l_1 = 50$  mm of the proximal phalanx,  $BD' = 25$  mm is chosen as a half. Since the proximal phalanx is rotated on ground joint  $B$  in the first mechanism layer,  ${}^o\theta_1 = 0$  and  ${}^e\theta_1 = -\delta\psi_{1B}$ .  $\delta\psi_{2D'}$  is predetermined to be  $140^\circ$  by considering the transmission ratio. The eccentric length of  $l'_{2B}$  is assumed to be collinear with the input link  $l_{2B}$ , and thus  $L_{2B} = l'_{2B} + l_{2B}$ . If  $l'_{2B}$  and  ${}^o\psi_{2D'}$  are designed so as to satisfy (20), then the transmission defect can also be estimated by using the following equation:

$$z' = \frac{1}{\delta\psi_{2B}} \int_{{}^o\psi_{2B}}^{{}^e\psi_{2B}} \cos^2 u_{E2} d\psi_{2B} \quad (21)$$

where

$$u_{E2} = \cos^{-1} \left( \frac{l_{2C'}^2 + l_{2D'}^2 - L_{2B}^2 - (l_1/2)^2 + l_1 L_{2B} \cos\psi_{2B}}{2l_{2C'}l_{2D'}} \right).$$

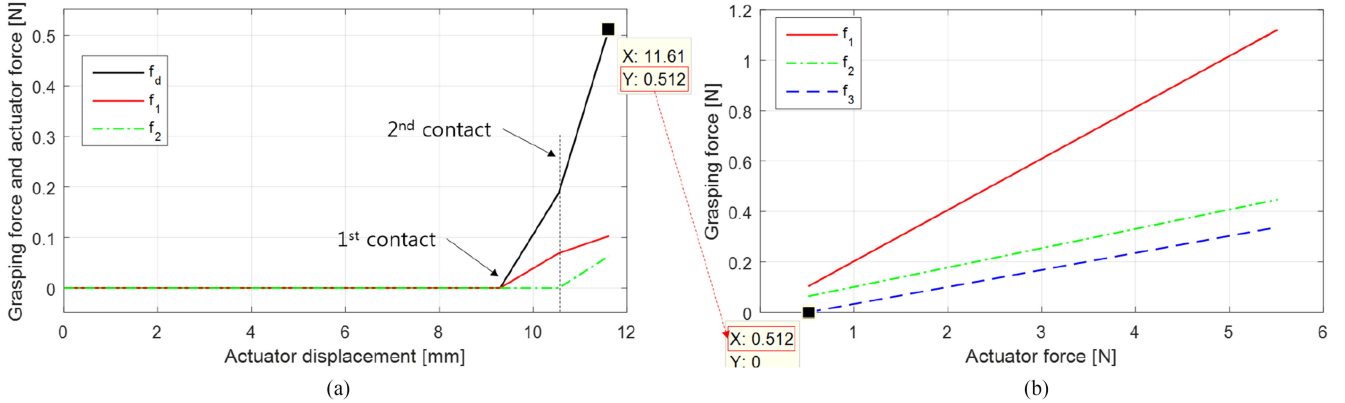


Fig. 8. Grasping forces distributed to the cylindrical object: (a) during contact; and (b) after contact.

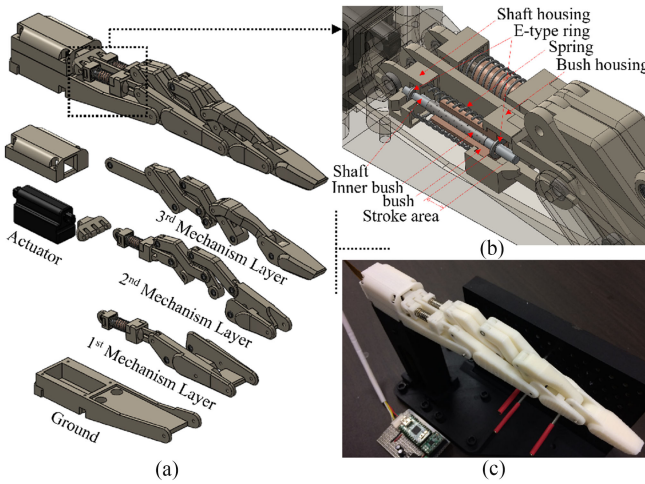


Fig. 9. Prototype design of the proposed robotic finger: (a) 3-D CAD model; (b) cross-sectional view on the coupler link in the first mechanism layer; and (c) prototype manufactured by a 3-D printer.

Fig. 6(c) shows contours of the transmission defect of the four-bar linkage  $BC'_2E_2D'$ , calculated from (21) according to various link lengths  $L'_{2B}$  and the initial output angles  ${}^o\psi_{2D'}$ . If we choose  $z' = 0.3255$ , then we can find all the design parameters, namely  $l_{2C'} = 38.38$  mm,  $l_{2D'} = 10.86$  mm,  ${}^o\psi_{2D'} = 135^\circ$ , and  $L'_{2B} = 25$  mm.

For another four-bar linkage  $D'E'_2F_2D$ , referring to Fig. 3 and (6) for  $i = 2$ , the previously designed parameters  $l_{2D'}$ ,  ${}^o\psi_{2D'}$ , and  $\delta\psi_{2D'}$  are used as its input. Let us replace the joint set of  $B$ ,  $C'_2$ ,  $E_2$ , and  $D'$  with  $D'$ ,  $E'_2$ ,  $F_2$ , and  $D$ , respectively, in Fig. 5(b).  ${}^o\psi_{2D}$  and  $\delta\psi_{2D}$  are predetermined as  $140^\circ$  and  $180^\circ$  to secure the ROM of the middle phalanx, respectively. After defining the corresponding Freudenstein's equation, the transmission defect is evaluated according to various  $L_{2D'}$  and  ${}^o\psi_{2D}$ , as shown in Fig. 6(d). If we choose  $z' = 0.2512$ , then all the design parameters are determined as  $l_{2E'} = 34.46$  mm,  $l_{2D} = 12.52$  mm,  ${}^o\psi_{2D} = 140^\circ$ , and  $L'_{2D'} = 25$  mm. As a result, Table I summarizes the initial and range of output angles used for the linkage design in all the mechanism layers. By using the data in Table I, all the lengths of the linkages are designed as suggested in Table II.

## V. SIMULATIONS AND EXPERIMENTS

### A. Natural Motion

In natural motion, the finger acts like 1 DOF coupled mechanism because the spring-loaded links  $l_{1A}$  and  $l_{2A}$  are supposed to be rigidly fixed as the initial values defined in Table II. The springs are assumed to have the same stiffness  $k_1 = k_2 = 0.157$  N/mm. Fig. 7 shows the simulation results for the natural motion. As joint  $A$  is translated from 0 to 20 mm, the natural motion sequence is conducted. The proximal, middle, and distal phalanges are concurrently rotated on joints  $B$ ,  $D$ , and  $G$ , respectively, as shown in Fig. 7(a). If (1) is applied to the proposed mechanism, we can confirm the approximate linear relationships between  $\theta_1$  and  $\theta_2$  as well as between  $\theta_1$  and  $\theta_3$  from Fig. 7(b) and (c). These linear relationships hold from  $0^\circ$  to  $65^\circ$  of the proximal angle with  $\lambda_1 = 1.7176$  and  $\lambda_2 = 2.2313$ . Also, we can know that the proximal, middle, and distal phalanges are rotated from the  $X_0$  axis to  $90^\circ$ ,  $180^\circ$ , and  $270^\circ$ , respectively, while the input displacement  $r$  moves from 0 to 20 mm by the linear actuator. In addition, we can confirm that the proposed finger mechanism is able to realize natural movement.

### B. Grasping Motion

A cylindrical object is grasped as a typical example of grasping motion. The center position of the cylinder with radius  $R = 25$  mm is fixed on the position  $x = 67$  mm and  $y = -50$  mm from origin  $O$ . When joint  $A$  connected to the linear actuator moves from 0 to 11.62 mm, the grasping sequences are completed, as animated in Fig. 7(d). Before the first contact between the proximal phalanx and the object, preshaping is generated with one DOF. When the proximal phalanx makes the first contact with the object, the proximal angle  $\theta_1$  stops rotating while  $\theta_2$  and  $\theta_3$  continue rotating, and also link  $l_{1A}$  having a linear spring starts to contract, as shown in Fig. 7(e) and (f). After the second contact, the middle phalanx also stops rotating, both links  $l_{1A}$  and  $l_{2A}$  are contracted at the same time, and finally, the distal phalanx approaches the third contact, as shown in Fig. 3(d) and (f).

The grasping force can be calculated from (17). Fig. 8 shows the grasping force profiles at all the phalanges during the

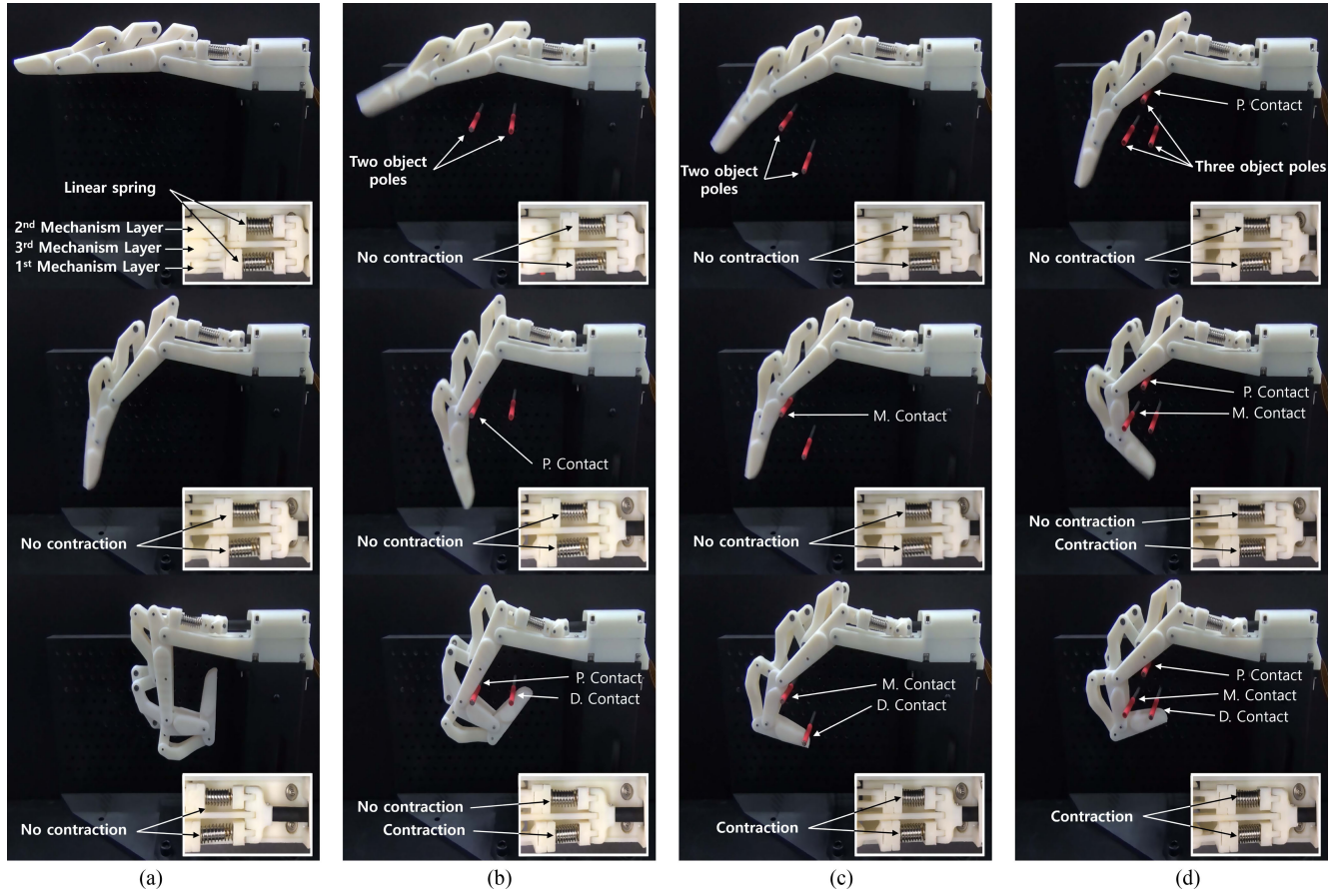


**Fig. 10.** Human-like natural motion and three types of self-adaptive grasping motions: (a) natural motion with one DOF without any contact; (b) self-adaptive grasping with two DOFs with proximal and distal contact; (c) self-adaptive grasping with two DOFs with middle and distal contact; and (d) self-adaptive grasping with three DOFs with proximal, middle, and distal contact.

grasping suggested in Fig. 7(d). Fig. 8(a) shows the grasping force profiles at the contact points in the proximal and middle phalanges just until the distal phalanx makes contact with the object. As soon as the proximal phalanx makes the first contact with the cylindrical object,  $f_1$  starts to increase by means of the spring embedded in the first mechanism layer. After the second contact with the middle phalanx,  $f_2$  is increased. For these, the actuator force  $f_d$  should be increased so as to generate the contact forces, as shown in the Fig. 8(a). After the distal phalanx makes contact, the grasping posture becomes static. Two springs are deformed as  $\delta l_{1A} = 2.2765$  mm and  $\delta l_{2A} = 1.0584$  mm, and thus the final angles of the phalanges are stuck at  $\theta_1 = -42.6027^\circ$ ,  $\theta_2 = -88.9706^\circ$ , and  $\theta_3 = -164.3460^\circ$ . The contact distances become  $h_1 = 39.2938$  mm,  $h_2 = 10.7062$  mm, and  $h_3 = 19.2925$  mm. In the static configuration, all the contact forces are directly related to the driving actuator force. The input force  $f_d$  starts to increase from 0.512 to 5.5 N, and then the grasping forces are distributed and increased, as shown in the Fig. 8(b). However, this does not imply that the finger can always grasp various objects stably since the grasping forces depend upon the posture (or configuration) of the finger mechanism.

### C. Experiments

The prototype, shown in Fig. 9, was designed and manufactured using Table II. The stack of three mechanism layers can

be decomposed, as shown in Fig. 9(a). In contrast, when all the layers are tied together around common joints, the stacked mechanisms complete the prototype. Fig. 9(b) illustrates a detailed cross-sectional view of the coupler link and the linear spring. The shaft and bush in their housings are fixed by an E-type snap ring. The bush housing has a space for the shaft to linearly move, and its movement is limited by the E-type snap ring. The linear spring is installed between both housings. The springs in the first and second mechanism layers have the same stiffness  $k = 0.157$  N/mm, which is identical to the one used for simulation in the previous section. Its no-load length and the maximal contractile lengths are 32 and 20.6 mm, respectively. The springs of the first and second mechanism layers have the preloaded lengths of 16.4 and 14.4 mm, respectively, in order to maintain tension during natural motion. The preloaded springs have the displacements of 5 and 3 mm, respectively.

The linear actuator was PQ-12 (manufactured by Firgelli Technologies Inc.) with the following specifications: a stroke of 20 mm, peak efficiency of 20[N] at 8 mm/s, no-load speed of 10 mm/s, and weight of 15 g. This provides the driving force  $f_d$  with the phalanges through three slider-cranks. The human finger-like natural motion was tested first. As demonstrated in Fig. 10(a), when the linear actuator is working, all phalanges are flexed as if it is a 1 DOF system due to the tension of the preloaded springs. Thus, all the coupler links

between the slider and the crank become stiff and are not contracted during the natural motion. Even when the linear actuator moved backward, the finger performed the extension motion well.

The finger was tested with static object poles to confirm the self-adaptive grasping motion. The object poles were fixed to arbitrary sites in a testbed wall, and then they were grasped by the phalanges. The linear actuator is actuated until the distal phalanx makes contact. Fig. 10(b) shows photographs of the grasping sequence. The phalanges are flexed as if exhibiting natural motion toward contact with the object poles. When the proximal phalanx makes the first contact with the object pole (P. Contact), it is constrained to stop flexion. The middle and distal phalanges continue being flexed because the spring in the first mechanism layer starts to be contracted. Here, the robotic finger acts like a 2 DOFs system. These motions of the phalanges are stopped when the distal phalanx is faced to the other pole (D. contact). In contrast, if the middle phalanx makes the first contact with the object pole (M. contact), then both the proximal and middle phalanges are stopped from being rotated at the same time, as shown in Fig. 10(c). In this situation, if the linear actuator continues working, two springs start to be simultaneously contracted and the distal phalanx moves toward contact with the other pole (D. contact). Finally, full grasping motion was conducted by using three object poles, as demonstrated in Fig. 10(d). After the proximal phalanx makes contact with the object pole, both the middle and distal phalanges are rotated with contraction of the spring in the first mechanism layer. Sequentially, the middle phalanx is faced to another object pole, and then the other spring in the second mechanism layer starts to be contracted as well. The distal phalanx moves toward contact with the other pole and finally the finger grasps the three poles substantially. Now, we can confirm that the finger has the ability to realize the natural motion as well as self-adaptive grasping.

## VI. CONCLUSION

This paper has presented an underactuated finger mechanism for implementing 3 DOFs motion with only one linear actuator and two springs. The aim was to design a robotic finger able to perform not only natural motion but also self-adaptive grasping. In particular, the natural motion was specified by three properties and it was shown that the proposed finger mechanism was able to satisfy them. Kinematics and statics were analyzed to reveal the operation principle of the proposed finger mechanism. Using static force analysis, we could confirm that the grasping forces were distributed and increased as all the phalanges were in contact with the object. The prototype of the robotic finger was designed and manufactured, and finally, its effectiveness was verified through several experiments. Further works is planned for practical use including, for example, selecting the stiffness regarding all the fingers, and developing a dynamic model that is able to justify the control system design for grasping and manipulation applications. Finally, we are planning to design and manufacture a multifingered robotic hand based

on the proposed finger mechanism, and ultimately, a bionic hand.

## REFERENCES

- [1] S. C. Jacobsen, E. K. Iversen, D. Knutti, R. Johnson, and K. Biggers, "Design of the Utah/MIT dexterous hand," in *Proc. IEEE Int. Conf. Robot. Autom.*, 1986, pp. 1520–1532.
- [2] F. Lotti, P. Tiezzi, G. Vassura, L. Biagiotti, G. Palli, and C. Melchiorri, "Development of UB hand 3: Early results," in *Proc. IEEE Int. Conf. Robot. Autom.*, 2005, pp. 4488–4493.
- [3] I. Yamano and T. Maeno, "Five-fingered robot hand using ultrasonic motors and elastic elements," in *Proc. IEEE Int. Conf. Robot. Autom.*, 2005, pp. 2673–2678.
- [4] A. D. Deshpande *et al.*, "Mechanisms of the anatomically correct testbed hand," *IEEE/ASME Trans. Mechatronics*, vol. 18, no. 1, pp. 238–250, Feb. 2013.
- [5] M. Grebenstein *et al.*, "The DLR hand arm system," in *Proc. IEEE Int. Conf. Robot. Autom.*, 2011, pp. 3175–3182.
- [6] N. E. N. Rodríguez, G. Carboné, and M. Ceccarelli, "Optimal design of driving mechanism in a 1-DOF anthropomorphic finger," *Mech. Mach. Theory*, vol. 41, no. 8, pp. 897–911, 2006.
- [7] N. Dechev, W. Cleghorn, and S. Naumann, "Multiple finger, passive adaptive grasp prosthetic hand," *Mech. Mach. Theory*, vol. 36, no. 10, pp. 1157–1173, 2001.
- [8] D. D. Didrick, "Articulated artificial finger assembly," U.S. Patent 6908489, Jun. 21, 2005.
- [9] T. Laliberté and C. M. Gosselin, "Simulation and design of underactuated mechanical hands," *Mech. Mach. Theory*, vol. 33, no. 1, pp. 39–57, 1998.
- [10] L. Birglen, T. Laliberté, and C. Gosselin, *Underactuated Robotic Hands*. New York, NY, USA: Springer, 2008.
- [11] B. Belzile and L. Birglen, "Stiffness analysis of underactuated fingers and its application to proprioceptive tactile sensing," *IEEE/ASME Trans. Mechatronics*, vol. 21, no. 6, pp. 2672–2681, Dec. 2016.
- [12] T. Laliberté, L. Birglen, and C. M. Gosselin, "Underactuation in robotic grasping hands," *Mach. Intell. Robot. Control*, vol. 4, no. 3, pp. 1–11, 2002.
- [13] D. Hirano, K. Nagaoka, and K. Yoshida, "Design of underactuated hand for caging-based grasping of free-flying object," in *Proc. IEEE/SICE Int. Symp. Syst. Integr.*, 2013, pp. 436–442.
- [14] G. Jang, C. Lee, H. Lee, and Y. Choi, "Robotic index finger prosthesis using stackable double 4-BAR mechanisms," *Mechatronics*, vol. 23, no. 3, pp. 318–325, 2013.
- [15] H. Lee, Y. Oh, W. H. Shon, and Y. Choi, "Stackable manipulator for mobile manipulation robot," in *Proc. IEEE Int. Conf. Robot. Autom.*, 2012, pp. 1964–1969.
- [16] H. Lee, Y. Choi, and B. J. Yi, "Stackable 4-BAR manipulators for single port access surgery," *IEEE/ASME Trans. Mechatronics*, vol. 17, no. 1, pp. 157–166, Feb. 2012.
- [17] M. Higashimori, M. Kaneko, and M. Ishikawa, "Dynamic preshaping for a robot driven by a single wire," in *Proc. IEEE Int. Conf. Robot. Autom.*, 2003, vol. 1, pp. 1115–1120.
- [18] G. Figoliini and M. Ceccarelli, "A novel articulated mechanism mimicking the motion of index fingers," *Robotica*, vol. 20, no. 1, pp. 13–22, 2002.
- [19] I. A. Kapandji, *The Physiology of the Joints*. Edinburgh, Edinburgh, Scotland: Churchill Livingstone, 1998 [Quoted in: G. Stillfried, U. Hillenbrand, M., Settles, and P. van der Smagt, "MRI-based skeletal hand movement model," in *The Human Hand as an Inspiration for Robot Hand Development*. New York, NY, USA: Springer, 2014, pp. 49–75].
- [20] G. Stillfried, U. Hillenbrand, M. Settles, and P. van der Smagt, "MRI-based skeletal hand movement model," in *The Human Hand as an Inspiration for Robot Hand Development*. New York, NY, USA: Springer, 2014, pp. 49–75.
- [21] L. Birglen and C. M. Gosselin, "Kinetostatic analysis of underactuated fingers," *IEEE Trans. Robot. Autom.*, vol. 20, no. 2, pp. 211–221, Apr. 2004.
- [22] F. Freudenstein, "An analytical approach to the design of four-link mechanisms," *Trans. ASME*, vol. 76, no. 3, pp. 483–492, 1954.
- [23] C. M. Gosselin, "Kinematic Analysis, Optimization and Programming of Parallel Robotic Manipulators," Ph.D. thesis, Dept. Mech. Eng., McGill Univ., Montréal, QC, Canada, Jun. 15, 1988.



**Dukchan Yoon** (S'16) was born in Seoul, South Korea, in 1987. He received the B.S. degree in electronic systems engineering from Hanyang University, Ansan, South Korea, in 2014, and the M.S. degree in electronic systems engineering and robotics from Hanyang University, Seoul, in 2016. Since 2016, he has been working toward the Ph.D. degree with Hanyang University.

His research interests include biorobotics, underactuated systems, mechanisms, and kinematics.



**Youngjin Choi** (SM'11) was born in Seoul, South Korea, in 1970. He received the B.S. degree in precision mechanical engineering from Hanyang University, Seoul, in 1994, and the M.S. and Ph.D. degrees in mechanical engineering from Pohang University of Science and Technology (POSTECH), Pohang, South Korea, in 1996 and 2002, respectively.

Since 2005, he has been a Professor with the Department of Electronic Systems Engineering, Hanyang University, Ansan, South Korea. From 2002 to 2005, he was a Senior Research Scientist at the Intelligent Robotics Research Center, Korea Institute of Science and Technology, Seoul, South Korea. From 2011 to 2012, he was a Visiting Researcher at the University of Central Florida, Orlando, FL, USA. His research interests include biorobotics, control theory, rehabilitation robots, and dual-arm manipulation.

Dr. Choi was an Associate Editor of the IEEE TRANSACTIONS ON ROBOTICS from 2010 to 2014. Since 2015, he has been an Associate Editor of the IEEE ROBOTICS AND AUTOMATION LETTERS.